

Kinesin Recycling in Stationary Membrane Tubes

Paige M. Shaklee,^{†§} Timon Idema,[‡] Line Bourel-Bonnet,[¶] Marileen Dogterom,^{§*} and Thomas Schmidt^{†*}

[†]Physics of Life Processes, [‡]Lorentz Institute, Leiden Institute of Physics, Leiden University, Leiden, The Netherlands; [§]FOM Institute for Atomic and Molecular Physics (AMOLF), Amsterdam, The Netherlands; and [¶]Equipe de Biovectorologie, Laboratoire de Conception et Application des Molécules Bioactives, UMR 7199 Centre National de la Recherche Scientifique/ Université de Strasbourg, Faculté de Pharmacie, Illkirch, France

ABSTRACT Collections of motors dynamically organize to extract membrane tubes. These tubes grow but often pause or change direction as they traverse an underlying microtubule (MT) network. In vitro, membrane tubes also stall: they stop growing in length despite a large group of motors available at the tip to pull them forward. In these stationary membrane tubes in vitro, we find that clusters of processive kinesin motors form and reach the tip of the tube at regular time intervals. The average times between cluster arrivals depends on the time over which motors depart from the tip, suggesting that motors are recycled toward the tip. Numerical simulations of the motor dynamics in the membrane tube and on the MTs show that the presence of cooperative binding between motors quantitatively accounts for the clustering observed experimentally. Cooperative binding along the length of the MT and a nucleation point at a distance behind the tip define the recycling period. Based on comparison of the numerical results and experimental data, we estimate a cooperative binding probability and concentration regime where the recycling phenomenon occurs.

INTRODUCTION

Transportation within the cell is driven by mechanoenzymes: motor proteins (1). Motors are responsible for cargo transport and continuous reorganization of membrane compartments. Because of their essential cellular function, the physical properties of individual motor proteins have been heavily investigated. Details on how individual motors function, however, are not sufficient to explain intracellular transport phenomena. Increasing evidence suggests that cooperation between multiple motors is critical for regulating cargo transport in cells (2–5). To date, our understanding of how motors behave collectively is still limited.

Collective motor dynamics have been previously studied with a minimal model system where kinesin motors are attached to giant unilamellar vesicles (GUVs) (6,7). When the motor-coated GUVs encounter a surface decorated by microtubules (MTs), the motors walk on the MTs and extract membrane tubes from the GUV (8). Because a single motor can only provide ≈ 5 pN of force (9), and membrane tube extraction requires ≈ 20 – 30 pN (10,11), motors dynamically associate at the tips of membrane tubes to share the tube-pulling load (8,12). Collective motor dynamics have primarily been studied in continuously growing membrane tubes. However, in vivo, membrane tubes can be seen pausing and changing direction regularly (see movie of membrane tubes in vivo (13)). To our knowledge, dynamics of motor proteins in membrane tubes that are paused have not yet been investigated.

In this article, we examine the dynamics of processive kinesin motors in stalled membrane tubes in vitro. We find

that motors repeatedly congregate en route to the tip of the membrane tube. Once arrived at the tip, motor clusters dissolve and subsequently reappear along the membrane tube at regular time intervals. Moreover, we find that the average time for clusters to form depends on the time over which motors depart from the tip. We explain the clustering phenomenon by cooperative binding, where binding next to a motor that is already bound to the MT is easier than binding to an unpopulated area of the MT. With a simple one-dimensional lattice model, we are able to reproduce the motor dynamics with numerical simulations. Simulations that account for cooperative binding reproduce the cluster formation found in experiments. If, moreover, we assume that motors cooperatively unbind at the tip of the membrane tube, and that a cluster nucleation point exists somewhere on the tube, the simulations also recover the relationship between average arrival time and tip decay time.

MATERIALS AND METHODS

GUVs

1,2-Dioleoyl-*sn*-glycero-3-phosphocholine (DOPC) was purchased from Avanti Polar Lipids (Alabaster, AL) and a rhodamine-labeled biotinylated phosphatidylethanolamine (Rh-B-DSPE) was acquired from Dr. Line Bourel-Bonnet (14). A lipid composition of 99.9 mol % DOPC with 0.1 mol % Rh-B-DSPE was used. The ratio of lipids was chosen so that a GUV of ~ 10 μm in diameter had ~ 100 biotin binding sites. A solution of 10 μL of 2 mM lipids in 1:10 chloroform/methanol was dropped onto one of two indium tin oxide-coated glass slides (4 cm \times 6 cm). The lipids were distributed on the glass by the rock-and-roll method (7) and dried for 1 h on a 50°C hotplate under continuous nitrogen flow. A 300- μL volume chamber was constructed from the two glass plates, the dried lipids on the bottom glass, and a polydimethylsiloxane spacer. The chamber was

Submitted December 9, 2009, and accepted for publication June 30, 2010.

*Correspondence: Schmidt@physics.leidenuniv.nl or dogterom@amolf.nl

Editor: Hideo Higuchi.

© 2010 by the Biophysical Society
0006-3495/10/09/1835/7 \$2.00

doi: 10.1016/j.bpj.2010.06.071

filled with a solution of 200 mM sucrose and an AC voltage applied to the glass plates, forming GUVs by the electroformation method (7).

MTs and motor proteins

Microtubules (MTs) were prepared from tubulin purchased from Cytoskeleton (Denver, CO). Tubulin (10 mg/mL) in MRB40 (40 mM PIPES, 4 mM MgCl₂, and 1 mM EGTA, at pH 6.8) with 1 mM GTP was incubated for 15 min at 37°C to polymerize. MTs were stabilized by mixing them 1:10 (vol/vol) with MRB40 containing 10 μM taxol (MRB40tax). Truncated and biotinylated kinesin-1 from *Drosophila melanogaster* was used. From the N- to C-terminus, the kinesin construct consists of the first 401 residues of the kinesin heavy chain (slightly modified from plasmid pEY4 (15)), followed by a triple hemagglutinin tag and finally a biotin carboxyl carrier protein for attachment of a biotin. Kinesins were expressed in *Escherichia coli*, purified as described in Young et al. (6), and further purified by microtubule affinity purification. Motors were tested for activity with a MT gliding assay where the motors were bound specifically to the glass via their biotin. MT gliding assays with both MRB40tax and MRB80tax (80 mM PIPES, 4 mM MgCl₂, and 1 mM EGTA, at pH 6.8) showed the same range of gliding speeds: 450 ± 50 nm/s.

Sample preparation

Glass coverslips were diethylenetriamine (DETA)-treated as described in Verbruggen et al. (16). A 15 μL flow cell with a glass slide, two thin lines of vacuum grease, and a DETA-treated coverslip was constructed. Taxol stabilized MTs incubated in the flow cell for 10 min to adhere to the surface. MTs that did not stick to the surface were removed by rinsing the flow cell twice with MRB40tax. Casein Sodium Salt (Sigma Aldrich, St. Louis, MO) (200 μg/mL) was incubated in the flow cell for 8 min to block the remaining surface and minimize interaction of GUVs with exposed glass. The flow cell was subsequently rinsed with MRB40tax.

GUVs were mixed 1:1 in MRB40tax with 180 mM glucose to osmotically match the intravesicular osmolarity (Halbmikro Osmometer, Type M; Knauer, Germany). One microliter of 2 mg/mL streptavidin was added to 30 μL of the vesicle solution (where the number of vesicles in the solution typically ranged from 200 to 700) and was incubated for 10 min. Next, 1 μL of 2 μM biotinylated kinesin was added and incubated for 10 min so that the kinesin could bind to the Rh-B-DSPE lipids via streptavidin.

It should be noted that streptavidin was added in excess of biotinylated-rhodamine lipids and remained in excess of biotinylated-kinesin to avoid artificial aggregation of motors. For example, a 10-μm vesicle had ≈ 100 rhodamine-biotin lipid binding sites and in any given sample, there were ≈ 1000 vesicles so there was, roughly, a maximum of 10⁵ biotin binding sites available on vesicles. A quantity of ≈ 10¹³ streptavidin molecules were incubated with the vesicles followed by ≈ 10¹² biotinylated kinesin molecules. Any fluorescent lipids, either with or without motors bound, that did not interact with an MT diffused so quickly (1 μm²/s (12,17)) that they only contributed an average background fluorescent signal.

As in Shaklee et al. (17), we further ruled out that artificial aggregation of lipid-motor complexes occurred by determining the spatial correlation of motors binding along the MT. In brief, we extended a line along the length of the membrane tube (but not extending into the vesicle or the tip region) and determined the intensity profile, $F(r)$, along this line. We then determined the normalized spatial autocorrelation, $H(\rho)$, where

$$H(\rho) = \frac{\langle F(r + \rho)F(r) \rangle}{\langle F(r) \rangle^2}.$$

The spatial correlation for the fluorescent signal decayed to zero at the distance of the point-spread-function of the microscope, indicating that motors did not artificially aggregate or show preferential binding regions on the MT. Moreover, we expected that artificial motor aggregation would

result in persistently large fluorescence signals with a different diffusion constant than for individual motor-lipid complexes. In Shaklee et al. (17), fluorescence image correlation spectroscopy (temporal) and fluorescence recovery after photobleaching measurements, under the same assay conditions, confirmed the presence of a single diffusive species.

Finally, 0.5 μL Oxygen Scavenger (8 mM DTT, 0.4 mg/mL catalase, 0.8 mg/mL glucose oxidase) and 1 μL of 100 mM ATP were added to the vesicle solution leading to a total vesicle solution volume of ≈ 33.5 μL and final ATP concentration of ≈ 3 mM. Fifteen microliters of this vesicle solution was slowly pipetted with a cut-off pipette tip into the flow cell. The flow cell was sealed with nail polish at the open ends.

Image acquisition and analysis

Data was acquired on a spinning disk microscope comprised of a confocal scanner unit (CSU22; Yokogawa Electric, Tokyo, Japan) attached to an inverted microscope (DMIRB; Leica, Wetzlar, Germany) equipped with a 100×/1.3 NA oil immersion lens (PL FLUOTAR; Leica) and a built-in 1.5× magnification changer lens. The sample was illuminated using a 514-nm laser (Coherent, Santa Clara, CA). Images were captured by an electromagnetic charge-coupled device camera (C9100; Hamamatsu Photonics, Iwata-City, Japan) controlled by software from VisiTech International (Sunderland, UK). Images were acquired with a 100-ms exposure at 10 Hz. Spinning disk microscopy imaging was chosen to minimize bleaching effects.

Movies were analyzed using a home-written MATLAB (The MathWorks, Natick, MA) algorithm. The algorithm determines the intensity along the line (one-pixel-wide) of a membrane tube. This intensity is determined for the same line along the membrane tube for each image in the movie and the resulting change in intensities through time are presented in a kymograph. The algorithm also calculates the autocorrelation in the tip region, autocorrelation along the rest of the length of the tube and the power spectrum from the kymograph. The temporal autocorrelation for a single pixel is described as

$$G(\tau) = \frac{\langle F(t + \tau)F(t) \rangle}{\langle F(t) \rangle^2}.$$

The autocorrelation is calculated for each pixel along the membrane tube line (excluding the tip region) and the average autocorrelation from these curves is calculated. For ease of comparison between tubes, the tip region is defined as the three pixels at the very tip of the membrane tube, which is equivalent to ≈ 330 nm.

Numerical simulations

Monte Carlo simulations were written and executed in MATLAB using the parameters described in the text. We assumed a one-dimensional membrane tube and MT lattices. On the membrane tube, motors were allowed to occupy the same space, while on the MT lattice no more than one motor was allowed per lattice site. In the membrane tube, motors freely diffused in one dimension and encountered reflecting boundaries at either end of the lattice. On the MT, motors walked unidirectionally toward the tip where they encountered a hard boundary (a no-flow boundary condition). In each step, we checked that there was a sufficiently large motor cluster to hold the membrane tube at the tip; if the tip cluster was smaller than six motors, we terminated the simulation. Each lattice site was assumed to be 8 nm, corresponding to the size of a tubulin dimer. Each of the simulations was run for 72,000 time steps, corresponding to 1200 s. The simulations produced kymographs that were analyzed in the same way as the kymographs from the experimental data. Each of the simulation points in Fig. 5 was determined from the last 300 s of three different simulations. 300 s was chosen to be comparable to the experimental observation times.

RESULTS AND DISCUSSION

Motor recycling

We use a minimal *in vitro* model system, in which kinesin motors are specifically attached to fluorescently labeled lipids (14) in GUVs (7), to directly examine motor dynamics during membrane tube formation as described in the literature (12,17). When a motor-coated GUV encounters MTs on a glass surface, the kinesins collectively extract membrane tubes from the GUV as they walk on the underlying MTs (8,12). The motors accumulate at the tip of the growing membrane tube where their speeds are damped by the tube-pulling force (8,12). At some point, we observe that tubes stop growing, even though there is a large group of motors accumulated at their tip. There are two possible explanations for this halt in tube growth: either the motors have reached the end of their MT (or a MT defect or junction), or, as observed by Campàs et al. (18), the tube force balances the collective motor force. Although we occasionally find oscillating tubes like the ones reported by Campàs et al. (see [Movie S2](#) in the [Supporting Material](#)), we focus here only on the stationary ones.

[Fig. 1 a](#) shows the sum of a series of images of membrane tubes formed by kinesin motors. To visualize the motor dynamics, motors are bound to fluorescently labeled lipids in the membrane. The fluorescence signal appears wherever a lipid-motor complex is also bound to the MT. Fluorescent lipid-bound motors that are not interacting with the MT diffuse through the membrane on a timescale much faster than our imaging time, so they only contribute to an average background fluorescence signal. At and toward the right of the star symbol in [Fig. 1 a](#), the fluorescence rapidly decreases because the membrane tube is lifted from the surface and not anchored by motors to the MT. [Fig. 1 b](#) shows a schematic cartoon of the membrane tube, where X denotes the distance behind the tip at which the membrane tube lifts away from the MT.

Though the tube is stationary, motors are still highly active in the tip region (see [Movie S1](#), [Movie S2](#), and [Movie S3](#)), as indicated by fluctuations in the intensity of the fluorescent lipids that are specifically bound to motors (see [Materials and Methods](#)). We trace the motor positions through time as they walk toward the tip of the membrane

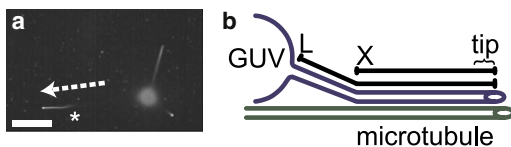


FIGURE 1 Kinesin dynamics in membrane tubes. (a) Membrane tubes formed by kinesin motors. The image is a sum of a series of images tracing kinesin-bound fluorescent lipids dynamics in a membrane tube network. The star indicates the point at which the membrane tube is connected to the underlying MT (MTs not visible). Scale bar, 5 μm . (b) Cartoon showing the geometry of a membrane tube of length L extending from a GUV. The tube is anchored to the MT a distance X behind the tip.

tube, in the direction of the dashed arrow as shown in the example in [Fig. 1 a](#) (corresponding to [Movie S1](#)). In the resulting kymograph ([Fig. 2 a](#)), we observe that the motors congregate to form clusters. The sum of the fluorescence signal from motor-bound lipids along the length of the membrane tube, both bound to the MT and freely diffusing, stays the same through time, varying by only 3%. The constant total fluorescent signal indicates that the average number of motors in the membrane tube is constant.

The motors in [Fig. 2 a](#) appear to accumulate and move toward the stationary tip at regular time intervals. We determine the length of these time intervals with the autocorrelation curve and power spectrum, averaged for all points along the tube, of the kymograph ([Fig. 2, c and d](#)). Both methods show that the arrivals are indeed periodically spaced. This result holds for all stationary tubes we have observed. We relate the periodicity of cluster arrival to the time it takes motor clusters to dissipate at the tip, as determined from the decay of the autocorrelation curve at the tip ([Fig. 2 e](#)). We define the tip region as the tip-most 0.33 μm of all membrane tubes. We verify that photobleaching is not the source of the loss of fluorescence at the tip of the membrane tube (see details in the [Supporting Material](#)). The motor decay times at the tip, scale linearly with the cluster arrival times ([Fig. 2 f](#)), where

$$t_{\text{decay}} = (0.97 \pm 0.05)t_{\text{arrival}}.$$

Each of the squares in [Fig. 2 f](#) represents a different membrane tube. Based on this observation, we suggest that the motors are recycled toward the tip. It should be noted that diffusion alone cannot account for the timescale of this recycling pattern: motors can diffuse a distance of 2 μm in <1 s (12,17).

To understand how motors form clusters, we examine the fluorescence density profile as motor-bound fluorescent lipids move toward the tip. Each time a motor cluster reappears, the motor density starts small and increases as the motors move toward the tip of the membrane tube, as indicated by an increase in the fluorescence intensity of a building cluster (following the *dashed line* in [Fig. 2 a](#) and shown in [Fig. 2 b](#)). Cluster formation can be explained by cooperative binding of the motors. Once a few motors have bound to the MT and walk toward the tip, motors diffusing in the membrane tube have a high probability of binding to the MT next to the motors already bound to the MT. This cooperative binding could simply arise from an increased proximity of the membrane tube to the MT lattice, making it easier for motors to bind, or from a mutual interaction between motors (19,20).

Cooperative binding and a nucleation point

To explain the motor recycling pattern, we propose that motors diffusing in the membrane may randomly bind at

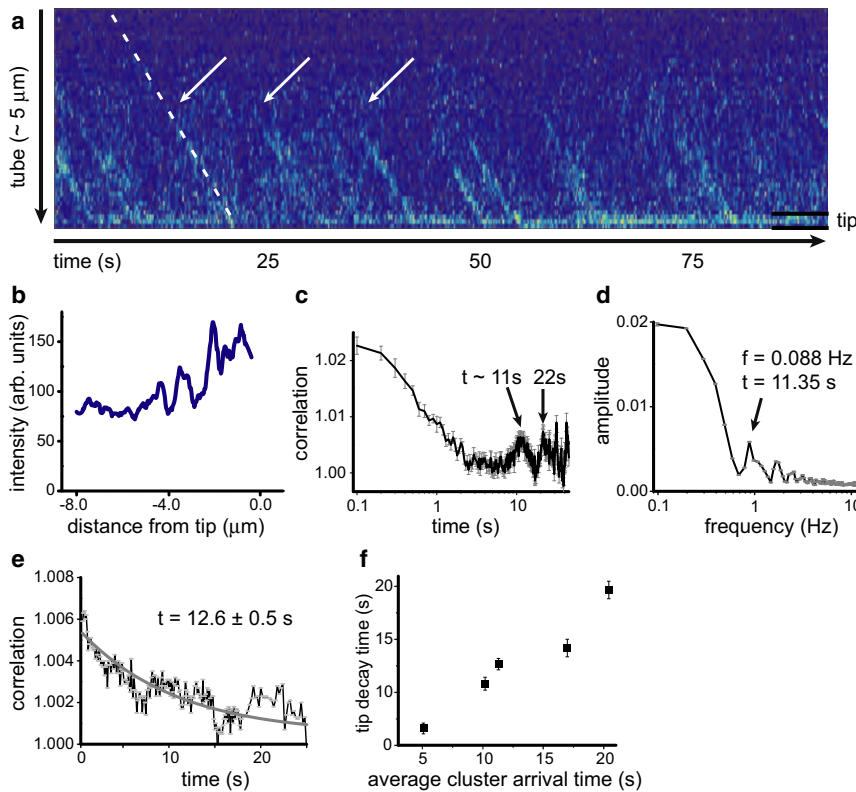


FIGURE 2 Motor cluster timescale. (a) Kymograph tracing the motor dynamics in the direction of the dashed arrow of Fig. 1 a in time. The arrows indicate examples of new kinesin motor clusters. The dashed line traces along a growing motor cluster as it moves to the tip. (b) Intensity profile following the dashed line in panel a. Approximately $5 \mu\text{m}$ behind the tip, motors begin to accumulate and the cluster grows as it reaches the tip of the membrane tube. (c) Autocorrelation curve in time, averaged for all points along the membrane tube of Fig. 1. The correlation curve shows distinct peaks at $\approx 11 \text{ s}$ and 22 s ($n = 18$). (d) The peak at $\sim 11 \text{ s}$ is confirmed by a peak in the power spectrum ($n = 18$). (e) The autocorrelation curve at the very tip of the membrane tube (the tip-most $0.33 \mu\text{m}$) is fit with an exponential decay. The decay time of this fit represents the time, $12.6 \pm 0.5 \text{ s}$, it takes for clusters at the tip to dissipate ($n = 33$). (f) Plot of the tip decay time versus the typical cluster arrival time for five individual tubes from different experiments. The times at which motor clusters form is linearly related to the release of motors from the tube where $t_{\text{decay}} = (0.97 \pm 0.05)t_{\text{arrival}}$.

a nucleation point a distance X behind the tube tip (cartoon in Fig. 3). Here X is defined by the average point at which a few motors anchor the membrane tube to the MT, as indicated by the star symbol in Fig. 1 a and shown in the cartoon in Fig. 1 b. We assume this point to be stationary over the timescales of our experimental measurements. This geometry has been observed experimentally (12) and corresponds to a shape that minimizes the energy of the GUV/membrane tube system by minimizing the curvature at the point where the tube meets the GUV (21,22).

We use Monte Carlo simulations to investigate whether a nucleation point and cooperative binding can account for the trends in our experimental data. We consider a MT

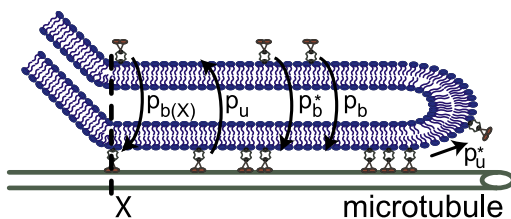


FIGURE 3 Model schematic. Motors bind randomly anywhere along the MT lattice with a probability p_b and a distance X behind the tip of the membrane tube with a probability $p_{b(X)}$. However, if a diffusing motor neighbors a motor that is already bound to the MT lattice, the diffusing motor will bind next to it on the MT with a probability p_b^* . Once on the MT lattice, motors may walk toward the tip of the MT or detach from the MT with a probability p_u and at the very tip with a probability p_u^* .

directly beneath a membrane tube with N motors. The high curvature of the membrane tube limits motor access to the MT (23), thus, we simulate the motor dynamics on a single protofilament and in a one-dimensional membrane tube. Motors in the membrane diffuse with diffusion constant D . They do not feel each other and may occupy the same lattice site. For a lipid-motor complex freely diffusing in a membrane tube, $D = 1.2 \pm 0.2 \mu\text{m}^2/\text{s}$ (12,17).

The cartoon in Fig. 3 shows the probabilities that govern motor dynamics in the membrane tube and on the MT in the simulations. Motors in the membrane tube randomly bind anywhere along the MT lattice with very small probability $p_b = 0.001$ per step (23), and at the nucleation point with probability $p_{b(X)} = 0.02$ per step. The value of p_b is small, because a motor is likely to diffuse in the membrane for a long time before encountering the MT below. This time is set by membrane tube fluctuations so that the majority of the lipid bilayer is not close to the MT (24). At X , the probability of binding is larger because the membrane tube is anchored there and hence closer to the MT. As soon as motors feel clusters on the MT below, they bind with a probability

$$p_b^* = \gamma p_{b(X)}.$$

We choose $\gamma = 12$ to account for the six neighboring binding sites per motor on an actual MT, where we assume that a minimum cluster is two motors (23). Once motors are bound to the MT, they walk toward the tip with velocity v , as

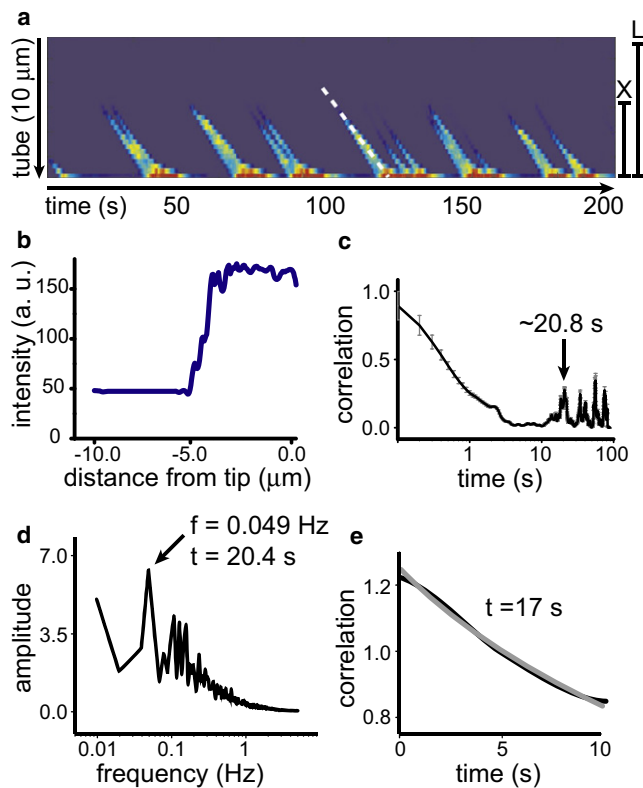


FIGURE 4 Simulations. (a) Kymograph from a simulation where motors bind cooperatively and with a nucleation point at X . Here $N = 100$, $L = 10 \mu\text{m}$, and $X = 5 \mu\text{m}$. Motor clusters appear approximately every 20 s. (b) Intensity profile tracing the growing cluster indicated by the dashed line in panel a. Motors begin to accumulate at the nucleation point $5 \mu\text{m}$ behind the tip. (c) Spatially averaged autocorrelation curve of the signal in panel a showing a distinct peak at $\approx 20.8 \text{ s}$ ($n = 15$). (d) Spatially averaged power spectrum of the signal with a peak at 20.4 s ($n = 15$). (e) Autocorrelation curve of the fluorescence signal at the tip of the membrane tube, fit with an exponential decay that gives a cluster dissipation time of 17 s ($n = 3$).

long as the site in front of it is unoccupied. Kinesin walks at speeds of $450 \pm 50 \text{ nm/s}$ (25,26). We account for this range of speeds in the simulations by assuming a Gaussian spread with a mean of $v \approx 53 \pm 7 \text{ steps/s}$. The assumption of a Gaussian spread results in a broader width of the fluorescence profile as a motor cluster builds toward the tip in the simulations, as seen in the kymograph of Fig. 4 a; the broadened width does not arise from cooperative binding. Kinesins walk on MTs for an average of 100 steps (27,28), so motors unbind from the lattice with probability $p_u = 0.01$ per step. At the tip of the tube crowding effects and the tube retraction force at the tip initially prevent the motors from stepping and thus from unbinding. However, as more motors arrive at the tip, the tip region gets increasingly crowded (20,29). Hence, the number of motors in the tip region that is frustrated in their attempts to walk forward also increases. The resulting buildup of motors unable to step occasionally results in a cascade effect in which a large amount of the motors in the tip cluster detaches. We observe

this detachment cascade in our experiments as an experimental decay in the autocorrelation curve of the motor number at the tip (Fig. 2 d). These cascade unbindings are rarer than regular unbindings, and increase in frequency as the density of motors at the tip increases; we therefore estimate the probability of unbinding to be

$$p_u^* = N \times p_u/100.$$

We use the above values for all the simulations.

Because the number of motors in a membrane tube, the length of a membrane tube, and the point where the tube is anchored to the MT are different in each experiment, we also vary these values in the simulations to see how the system responds. Based on our experimental conditions (see Materials and Methods), we expect $\sim 100 \text{ motors}/\mu\text{m}^2$ on any given vesicle and hence membrane tube. In our simulations, we use values of N between 25 and 120.

Tubes are held in place by motors at the tip that either stopped at the end of the MT or at an MT defect. The retraction force the tube exerts on the motors is $\approx 20\text{--}30 \text{ pN}$ (10,11), so that at least six motors (stall force per motor $\approx 5 \text{ pN}$ (9)) must be present at the tip to keep the tube in place. If fewer motors are present, they are pulled from the MT and the tube retracts. We terminate simulations with retractions because they no longer reflect the situation we intend to study, the stationary tubes (see Fig. S4, c and d). We find that a total number of 25 motors on the tube is just sufficient to maintain a large enough cluster at the tip in cases where the nucleation point is close to the tip. For even lower total motor numbers we find no stationary tubes at all; for higher motor numbers, we find stationary tubes for all values of X we consider. Tubes with >120 motors become very crowded at the tip and the dynamics of motor clusters can no longer be seen.

Note that N does not vary in an individual simulation because we assume the density of motors over the vesicle and tubes to be uniform. The results reported here are for tubes that range in total length from $5 \mu\text{m}$ to $10 \mu\text{m}$. Longer tubes show the same quantitative results as those of $10 \mu\text{m}$. The distance of the nucleation point from the tip (X) ranges from $2 \mu\text{m}$ to $7 \mu\text{m}$. Fig. 4 a shows a kymograph from a simulation where $N = 100$, $L = 10 \mu\text{m}$, and $X = 5 \mu\text{m}$. Fig. 4 b shows the intensity profile tracing a growing cluster (indicated by the dashed line in Fig. 4 a). As in the experimental case (Fig. 2 b), motors begin to accumulate in a cluster that grows toward the tip. The accumulation of motors in the simulated case appears to be much more rapid than in the experimental case; however, it should be noted that the noise present in the experimental case is not accounted for in the simulations. The kymograph, autocorrelation curve, power spectrum, and tip autocorrelation curve in Fig. 4, c–e, all show similar timescales of $\approx 20 \text{ s}$.

To determine whether the components and parameters in our simple model and simulations are necessary and/or

accurate, we probe motor cluster dynamics by removing the nucleation point and/or cooperative binding and by searching the parameter space of our simulations. In the absence of a nucleation point, motor clustering requires a much higher probability of cooperative binding and clusters do not arrive at regular time intervals (detailed analysis in Fig. S3). If cooperative binding is absent, both with and without a nucleation point, clusters do not even form (see Fig. S4). Even at high N , clusters do not form in the absence of cooperative binding. A reduced unbinding probability at the tip, which depends on the total motor number and general crowding effects, is also critical. When $p_u^* = p_u$, clustering does occur over regular time intervals, but the population of motors at the tip is not enough to continuously hold the membrane tip in place even at N as high as 60, a value in the middle of the expected range on a membrane tube. If we lower the unbinding probability at the tip to account for crowding effects alone, the linear relationship between arrival and decay times disappears (details in Fig. S5).

In the simulations in which we assume both cooperative binding and the presence of a nucleation point at X , we recover the experimentally observed dependence between arrival time and decay time for different values of N (see Fig. 4). The resulting average cluster arrival time versus the average decay time at the tip from simulations of different membrane tubes with varying X are shown in Fig. 5. We find that, for each value of N , an increase in X results in an increase in both the average decay time at the tip and the average cluster arrival time. The experimental data points, indicated by triangles in Fig. 5, fall into the

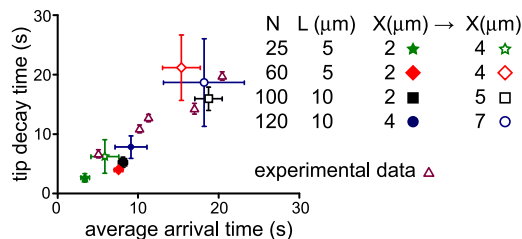


FIGURE 5 Average arrival time versus decay time at the tip from simulations. Scatterplot of simulated data for different motor number (N), length (L), and X . The different symbols represent different values of N . For fixed N , moving X to a position farther away from the tip (*open symbols* represent a larger X) results in an increase in timescales. The experimental data points (*triangles*) fall into the simulation regime. Error bars for the simulated data points are calculated based on accuracy of the correlation-curve fit as well as the variance between the different simulation values. The individual experimental data points, however, are each from a single membrane tube where the error only represents accuracy of the correlation-curve fit. The error bars are larger in the simulations than in the experimental data because each of the individual simulation points accounts for multiple simulations under the exact same motor number, tube length, and nucleation point conditions. The points with the largest error bars are from simulations where the nucleation point is far behind the tip. A nucleation point that is farther behind the tip takes longer for motors diffusing in the membrane tube to pass by, making the absolute time at which a new motor cluster starts to form more variable resulting in larger error bars.

same regime as the simulations for different values of N . Based on our simulation results, we suggest that motors in experiments are indeed recycled to make additional walking attempts to the membrane tube tip.

CONCLUSIONS

In conclusion, we have experimentally shown that motors in stationary membrane tubes spontaneously create a recycling pattern of motor clusters that grow as they move toward the tip of the tube at regular time intervals. Using Monte Carlo simulations, we have also shown that cooperative binding can account for the formation of motor clusters. Assuming a fixed point where the membrane tube meets the microtubule to be a nucleation point for motor clusters, we find a linear relationship between the average arrival time and tip decay time.

SUPPORTING MATERIAL

Four figures and three movies are available at [http://www.biophysj.org/biophysj/supplemental/S0006-3495\(10\)00842-8](http://www.biophysj.org/biophysj/supplemental/S0006-3495(10)00842-8).

The authors thank Drs. T. Surrey and F. Nédélec for the Kinesin plasmid, modified from pEY4 originally provided by Dr. J. Gelles; Dr. S. Olthuis-Meunier for protein purification; and Drs. K. Shundyak and P. R. ten Wolde for helpful discussions.

This work is part of the research program of the Stichting voor Fundamenteel Onderzoek der Materie, which is financially supported by the Nederlandse organisatie voor Wetenschappelijk Onderzoek within the program on Material Properties of Biological Assemblies (grant No. FOM-L1708M).

REFERENCES

- Howard, J. 2001. *Mechanics of Motor Proteins and the Cytoskeleton*. Sinauer, Sunderland, MA.
- Gross, S. P., M. A. Welte, ..., E. F. Wieschaus. 2002. Coordination of opposite-polarity microtubule motors. *J. Cell Biol.* 156:715–724.
- Hill, D. B., M. J. Plaza, ..., G. Holzwarth. 2004. Fast vesicle transport in PC12 neurites: velocities and forces. *Eur. Biophys. J.* 33:623–632.
- Kural, C., H. Kim, ..., P. R. Selvin. 2005. Kinesin and dynein move a peroxisome in vivo: a tug-of-war or coordinated movement? *Science*. 308:1469–1472.
- Klumpp, S., and R. Lipowsky. 2005. Cooperative cargo transport by several molecular motors. *Proc. Natl. Acad. Sci. USA.* 102:17284–17289.
- Young, E. C., E. Berliner, ..., J. Gelles. 1995. Subunit interactions in dimeric kinesin heavy chain derivatives that lack the kinesin rod. *J. Biol. Chem.* 270:3926–3931.
- Angelova, M. I., S. Soléau, ..., P. Bothorel. 1992. Preparation of giant vesicles by external AC fields. Kinetics and application. *Prog. Colloid Polym. Sci.* 89:127–131.
- Koster, G., M. VanDuijn, ..., M. Dogterom. 2003. Membrane tube formation from giant vesicles by dynamic association of motor proteins. *Proc. Natl. Acad. Sci. USA.* 100:15583–15588.
- Svoboda, K., C. F. Schmidt, ..., S. M. Block. 1993. Direct observation of kinesin stepping by optical trapping interferometry. *Nature*. 365:721–727.

10. Evans, E., and A. Yeung. 1994. Hidden dynamics in rapid changes of bilayer shape. *Chem. Phys. Lipids*. 73:39–56.
11. Koster, G., A. Cacciuto, ..., M. Dogterom. 2005. Force barriers for membrane tube formation. *Phys. Rev. Lett.* 94:068101–068104.
12. Leduc, C., O. Campàs, ..., J. Prost. 2004. Cooperative extraction of membrane nanotubes by molecular motors. *Proc. Natl. Acad. Sci. USA*. 101:17096–17101.
13. Waterman-Storer, C. M., and E. D. Salmon. 1998. Endoplasmic reticulum membrane tubules are distributed in living cells by three distinct microtubule dependent mechanisms. *Curr. Biol.* 8:798–806.
14. Jolimaître, P., A. Roux, ..., L. Bourel-Bonnet. 2005. Synthesis and preliminary physical applications of a rhodamine-biotin phosphatidylethanolamine, an easy attainable lipid double probe. *Chem. Phys. Lipids*. 133:215–223.
15. Berliner, E., E. C. Young, ..., J. Gelles. 1995. Failure of a single-headed kinesin to track parallel to microtubule protofilaments. *Nature*. 373:718–721.
16. Verbrugge, S., L. C. Kapitein, and E. J. G. Peterman. 2007. Kinesin moving through the spotlight: single-motor fluorescence microscopy with submillisecond time resolution. *Biophys. J.* 92:2536–2545.
17. Shaklee, P. M., L. Bourel-Bonnet, ..., T. Schmidt. 2010. Nonprocessive motor dynamics at the microtubule membrane tube interface. *Biophys. J.* 98:93–100.
18. Campàs, O., C. Leduc, ..., J. Prost. 2009. Collective oscillations of processive molecular motors. *Biophys. Rev. Lett.* 4:163–178.
19. Vilfan, A., E. Frey, ..., E. Mandelkow. 2001. Dynamics and cooperativity of microtubule decoration by the motor protein kinesin. *J. Mol. Biol.* 312:1011–1026.
20. Roos, W. H., O. Campàs, ..., G. Cappello. 2008. Dynamic kinesin-1 clustering on microtubules due to mutually attractive interactions. *Phys. Biol.* 5:046004.
21. Powers, T. R., G. Huber, and R. E. Goldstein. 2002. Fluid-membrane tethers: minimal surfaces and elastic boundary layers. *Phys. Rev. E Stat. Nonlin. Soft Matter Phys.* 65:041901.
22. Derényi, I., F. Jülicher, and J. Prost. 2002. Formation and interaction of membrane tubes. *Phys. Rev. Lett.* 88:238101.
23. Campàs, O., C. Leduc, ..., J. Prost. 2008. Coordination of Kinesin motors pulling on fluid membranes. *Biophys. J.* 94:5009–5017.
24. Fournier, J.-B., and P. Galatola. 2007. Critical fluctuations of tense fluid membrane tubules. *Phys. Rev. Lett.* 98:018103.
25. Shaklee, P. M., T. Idema, ..., M. Dogterom. 2008. Bidirectional membrane tube dynamics driven by nonprocessive motors. *Proc. Natl. Acad. Sci. USA*. 105:7993–7997.
26. Svoboda, K., P. P. Mitra, and S. M. Block. 1994. Fluctuation analysis of motor protein movement and single enzyme kinetics. *Proc. Natl. Acad. Sci. USA*. 91:11782–11786.
27. Thorn, K. S., J. A. Ubersax, and R. D. Vale. 2000. Engineering the processive run length of the kinesin motor. *J. Cell Biol.* 151:1093–1100.
28. Vale, R. D., T. Funatsu, ..., T. Yanagida. 1996. Direct observation of single kinesin molecules moving along microtubules. *Nature*. 380:451–453.
29. Frey, E., and A. Vilfan. 2002. Anomalous relaxation kinetics of biological lattice-ligand binding models. *Chem. Phys.* 284:287–310.